Supporting information

Effect of manganese porphyrin covalent immobilization on electrocatalytic water oxidation and oxygen reduction reactions

Aleksei N. Marianov[†] and Yijiao Jiang[†]*

[†]School of Engineering, Macquarie University, Sydney, NSW 2109, Australia

* To whom correspondence should be addressed:

Tel: +612-9850-9535

Fax: +612-9850-9128

E-mail: yijiao.jiang@mq.edu.au

Number of pages: 23

Number of figures: 21

Number of schemes: 3

Contents

1. Chemicals and materials

Chemicals were purchased from Sigma Aldrich and Alfa Aesar. Benzaldehyde and pyrrole were distilled under reduced pressure before use. Tetrabutylammonium hexafluorophosphate (TBAP) was recrystallized from ethanol and dried at 110 ºC. Anhydrous N,N-dimethylformamide (DMF) over molecular sieves was obtained from Ajax Finechem (purity > 99.9%; moisture content < 100 ppm). Carbon cloth was received from Fuel Cell Store. Flash column chromatography was performed on silica gel 70-230 mesh.

2. Additional methods and instrumentation

NMR spectroscopy

NMR spectra were recorded on Bruker Avance III 400 MHz spectrometer (Bruker). Chemical shifts were referenced against residual solvent peaks of $CDCl_3$.

Mass-spectrometry

ESI MS was recorded on Q Exactive™ Plus hybrid quadrupole-Orbitrap mass spectrometer (Thermo Fisher Scientific). 90 % acetonitrile with 0.1 % formic acid was used to dissolve sample of manganese (III) porphyrin.

IR spectroscopy

IR spectrum was recorded on Nicolet 6700 FT-IR spectrometer (Thermo Fisher Scientific) in the transmission mode with the sample pressed into KBr pellet.

UV-vis spectroscopy

UV-vis spectroscopy was performed on a single-beam HACH DR/4000 spectrometer (HACH) in a 10 mm quartz cuvette.

Thermogravimetric analysis

TGA/DSC STAR^e System (Thermo Fisher Scientific) was used for TGA analysis of carbon cloth based materials. 20 mL/min air flow and 2.5 ºC/min heating rate were used. Before each measurement blank TGA of an empty crucible was performed.

Stability studies

Stability of **MnTPP-noncov** and **MnTPP-cov/5** in OER was studied using 4 h long controlled potential electrolysis (CPE) in two-compartment electrochemical cell with chambers separated by porous glass frit under potential of 1.55 V vs NHE in 0.5 M H_2SO_4 electrolyte degassed with N_2. Analysis of gaseous products from anodic headspace was performed using Shimadzu GC 2014 gas chromatograph equipped with 6ft packed column and TCD detector using He as a carrier gas. Catalyst turnover frequencies (TOF) were calculated using equation 1.[1]

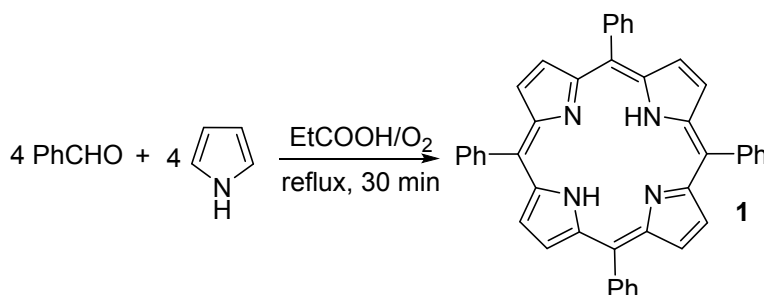$$TOF = \frac{(Q - Q_{bg})}{4Ft\Gamma_{EA}} \text{ (equation S1)}$$

Where (Q-Q_{bg}) is the charge passed during electrolysis with the background current corresponding to bare carbon cloth subtracted (C); F − Faraday's constant (C/mol); t − electrolysis duration (h); 4 − number of electrons transferred during water oxidation; Γ_{EA} − amount of electrochemically active catalyst per unit of electrode geometric surface area (mol/cm^2).

Stability of **MnTPP-cov/5** in ORR in alkaline medium was tested using prolonged CV experiment consisting of 500 cycles between -0.79 and 0.51 V vs NHE.

3. Synthesis of porphyrins

Meso-tetraphenylporphyrin (**1**)

Synthesis is based on the modified procedure reported by Adler et al.[2]

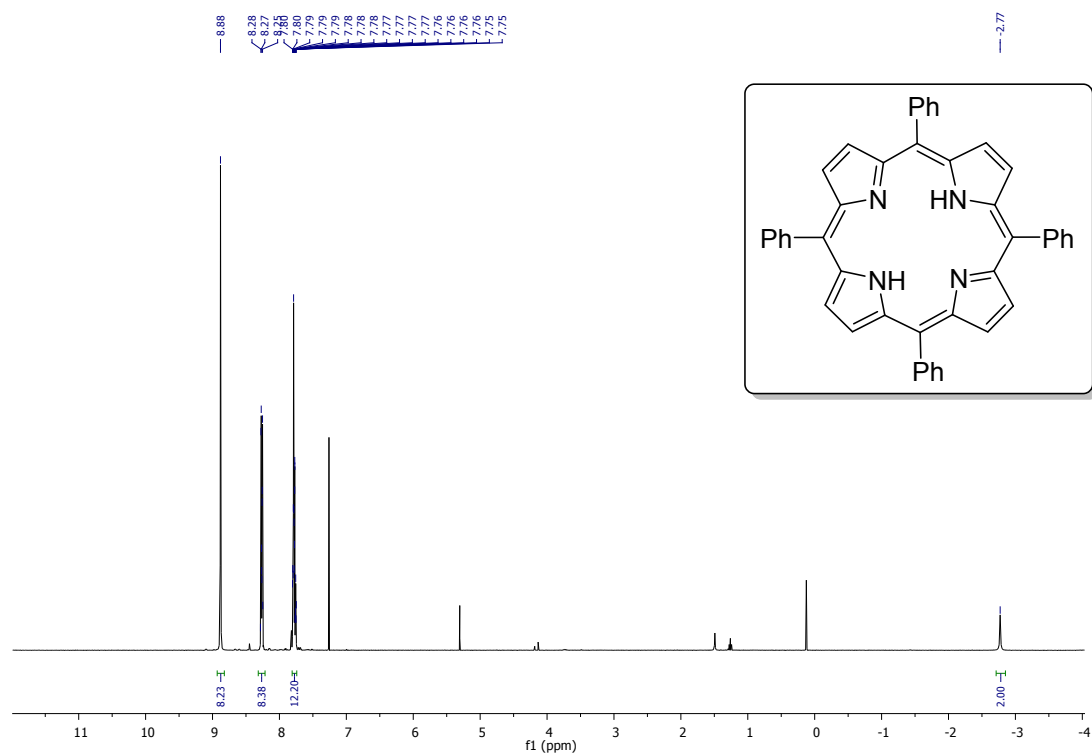**Scheme S1**. Synthesis of *meso*-tetraphenylporphyrin

Benzaldehyde (3.184 g, 30 mmol) and pyrrole (2.013 g, 30 mmol) were dissolved in 300 mL of propionic acid. Solution was refluxed under mild flow of oxygen for 30 min. 250 mL of acid were distilled off and 80 mL of methanol were added after cooling to the room temperature. Mixture was kept in the fridge overnight, precipitate was filtered off, washed with ethanol and dried. Reflux of the product in *n*-BuOH for 1 h, filtration and drying furnished pure, chlorin-free product in the form of violet crystalline substance (1.337 g, 29 %).

Note: purge of the system with oxygen increased the yield from 21 % to 29 % and simultaneously allowed to eliminate the formation of undesirable chlorin.
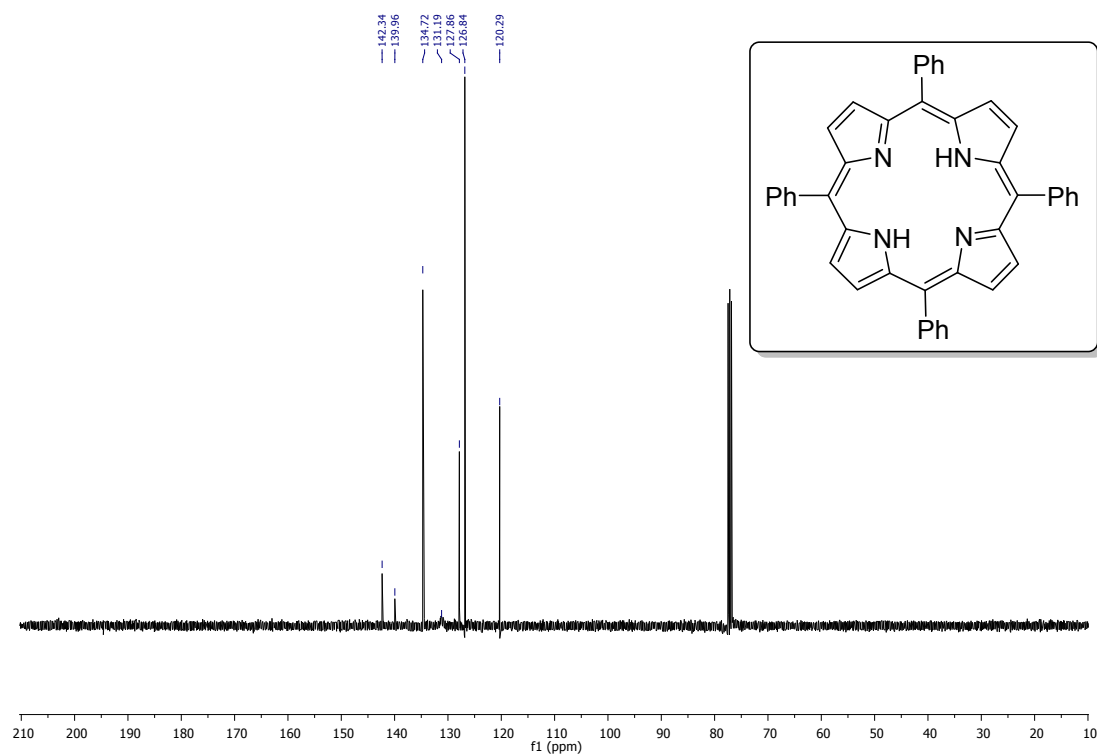
^{1}H NMR (400 MHz, CDCl$_3$) δ 8.88 (s, 8H), 8.28 − 8.25 (m, 8H), 7.80 − 7.75 (m, 12H), -2.77 (s, 2H) ppm

^{13}C NMR (100 MHz, CDCl$_3$) δ 142.3, 140.0, 134.7, 131.2, 127.9, 126.8, 120.3 ppm

Spectral data are in accordance with reported literature values.[3]
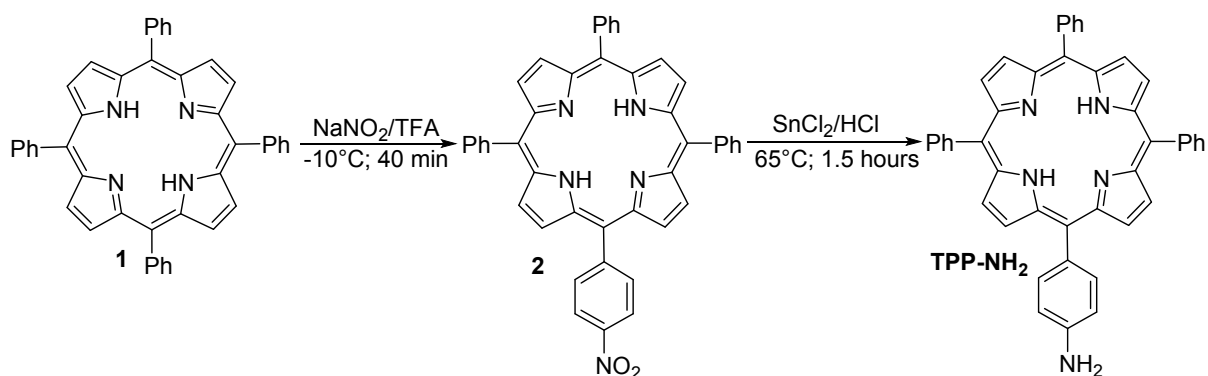
Figure S1. ¹H NMR spectrum of *meso*-tetraphenylporphyrin **1** (CDCl₃, 400 MHz).

Figure S2. ¹³C NMR spectrum of *meso*-tetraphenylporphyrin **1** (CDCl₃, 100 MHz).

5-(4-aminophenyl)-10,15,20-triphenylporphyrin (**TPP-NH₂**)

Synthesis is based on a modified procedure reported by Luguya et al.[4]

Scheme S2. Synthesis of 5-(4-aminophenyl)-10,15,20-triphenylporphyrin **TPP-NH₂**

a) Nitration.

Porphyrin **1** (615 mg; 1 mmol) was placed in a 100 mL round-bottom flask equipped with a magnetic stirring bar and dissolved in 50 mL of trifluoroacetic acid. Dark green solution was cooled to -10 ºC in an ice-salt bath. Sodium nitrite (104 mg; 1.5 mmol) was added in one portion. Solution quickly turned reddish-brown. Stirring was kept for 40 min, then the mixture was poured into 150 mL of water and carefully neutralized with K_2CO_3. Organic materials were extracted with dichloromethane (3 × 40 mL). Extracts were combined and dried over anhydrous Na_2SO_4. Solution was filtered, and its volume was reduced to ☐ 10 mL on the rotary evaporator. Liquid was transferred onto the pad of silica and porphyrins were separated with flash column chromatography. First fraction, containing unreacted **1** and 5-(4-nitrophenyl)-10,15,20-triphenylporphyrin **2** was eluted with CH_2Cl_2:PE (1:2).

b) Reduction.

Mixture of compounds **1** and **2** produced in the previous step was placed into a 100 ml round-bottom flask with a gas inlet, mixed with 50 mL of concentrated HCl and stirred for 30 min under mild flow of argon. Then $SnCl_2·2H_2O$ (814 mg, 3.6 mmol) was added in one portion and the temperature was increased to 65 ºC. Heating and stirring were kept for 1.5 h. Then the reaction mixture was cooled down to the room temperature and neutralized with NH_3 (30 % in

water) until pH reached □ 8. Resulting suspension was filtered under vacuum through 0.5 cm pad of SiO_2. Organics were washed down from the filter with CH_2Cl_2 directly into separatory funnel until washings turned colorless. Organic phase was washed with brine, dried over anhydrous Na_2SO_4, filtered and the solvent was removed under reduced pressure. Individual components of mixture were isolated using flash column chromatography (CH_2Cl_2:PE 1:3 → neat CH_2Cl_2). 0.124 mg of unreacted **1** were recovered along with aminoporphyrin **TPP-NH₂** (308 mg, 49 %).

Note 1: direct implementation of the published procedure at the room temperature led to the formation of a big amount of polynitrated products. Nitration at low temperature significantly improved its selectivity.[4]

Note 2: isolation of aminoderivative **TPP-NH₂** at the end of sequence is more feasible than the separation of porphyrins **2** and **1** due to bigger R_f difference.
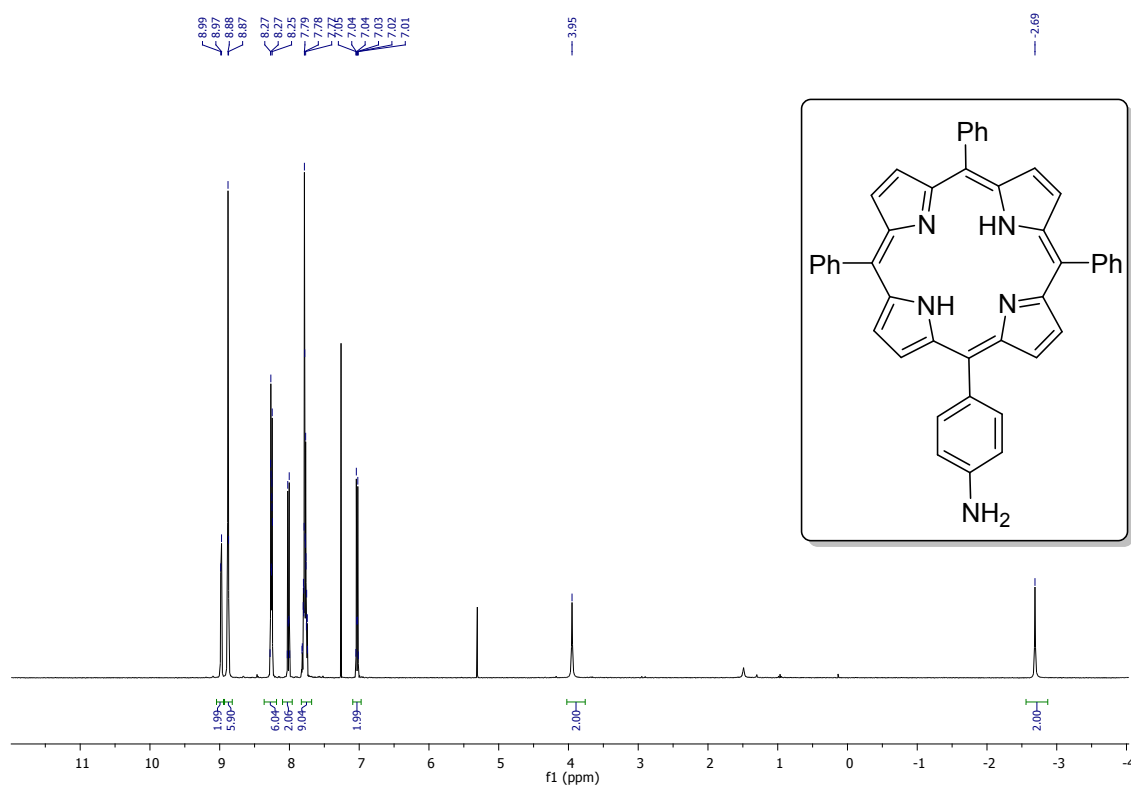
Note 3: reduction of **2** with $SnCl_2$ produces thick gunky precipitate of tin compounds floating in the interface of water and CH_2Cl_2 making simple extraction extremely cumbersome. Thus, filtration through a thin layer of silica or celite is recommended.

¹H NMR (400 MHz, $CDCl_3$) δ 8.98 (d, 2H), 8.88 – 8.87 (m, 6H), 8.28 – 8.24 (m, 6H), 8.03 – 8.00 (m, 2H), 7.82 – 7.74 (m, 9H), 7.05 – 7.01 (m, 2H), 3.95 (s, 2H), -2.69 (s, 2H) ppm

¹³C NMR (100 MHz, $CDCl_3$) δ 146.2, 142.4, 142.4, 135.8, 134.7, 132.5, 127.8, 126.8, 126.8, 121.0, 120.1, 119.9, 113.6 ppm
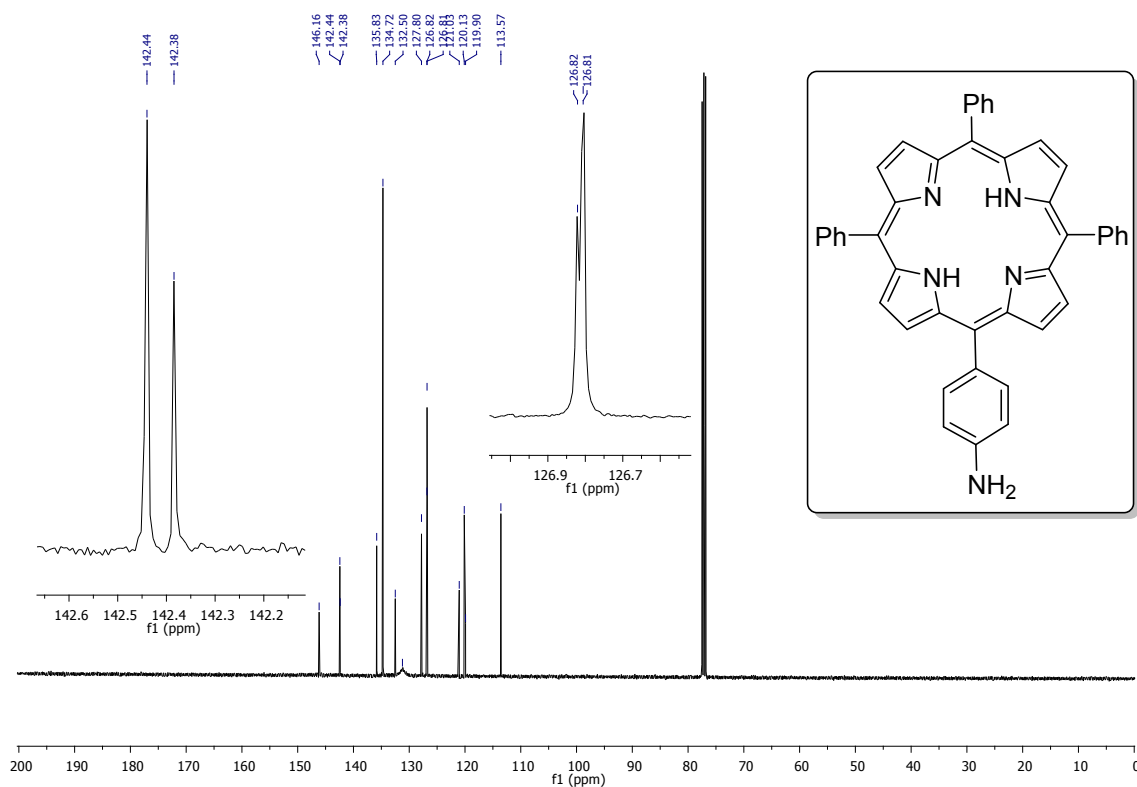
Spectral data are in accordance with reported literature values.[4]

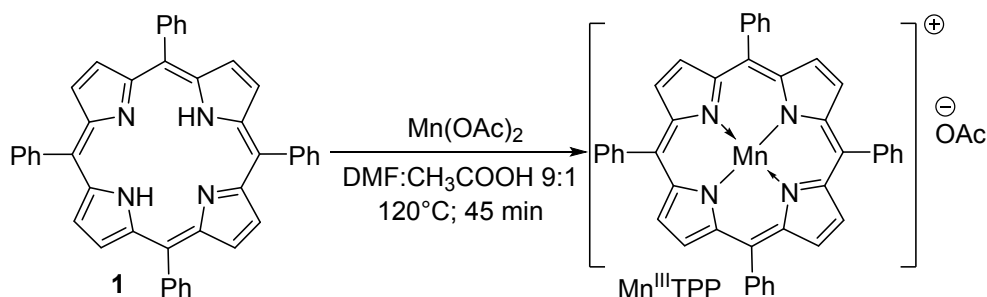**Figure S3**. ^{1}H NMR spectrum of 5-(4-aminophnenyl)-10,15,20-triphenylporphyrin

TPP-NH₂ (CDCl₃, 400 MHz).

Figure S4. ^{13}C NMR spectrum of 5-(4-aminophnenyl)-10,15,20-triphenylporphyrin

TPP-NH₂ (CDCl₃, 100 MHz).

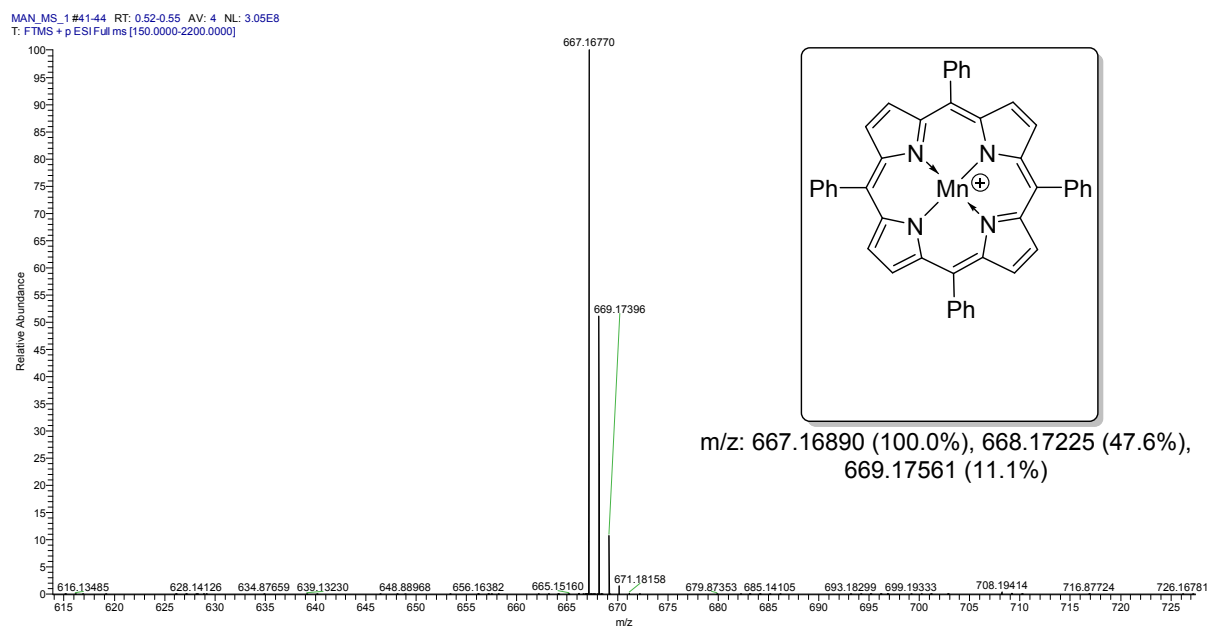*Manganese(III) meso-tetraphenylporphyrin acetate (MnTPP)*

Scheme S3. Synthesis of manganese (III) tetraphenylporphyrin acetate (MnTPP)

Tetraphenylporphyrin **1** (615 mg, 1 mmol) was dissolved in 30 ml of DMF:CH_3COOH (9:1) mixture at 120 ºC and manganese acetate tetrahydrate (1.226 g, 5 mmol) was added in one portion. Reaction mixture was stirred for 45 min and cooled down to the room temperature. Complex was precipitated from the solution by dropwise addition of water (60 mL) over the course of 1 h, filtered off, washed with deionized water and dried at 80 ºC overnight. Crude product was purified by column chromatography on silica gel (neat CH_2Cl_2 → 1:19 MeOH:CH_2Cl_2). Recrystallization from CH_2Cl_2:heptane via slow evaporation of solvent yielded complex MnTPP as greenish-black crystalline compound (311 mg, 43 %).

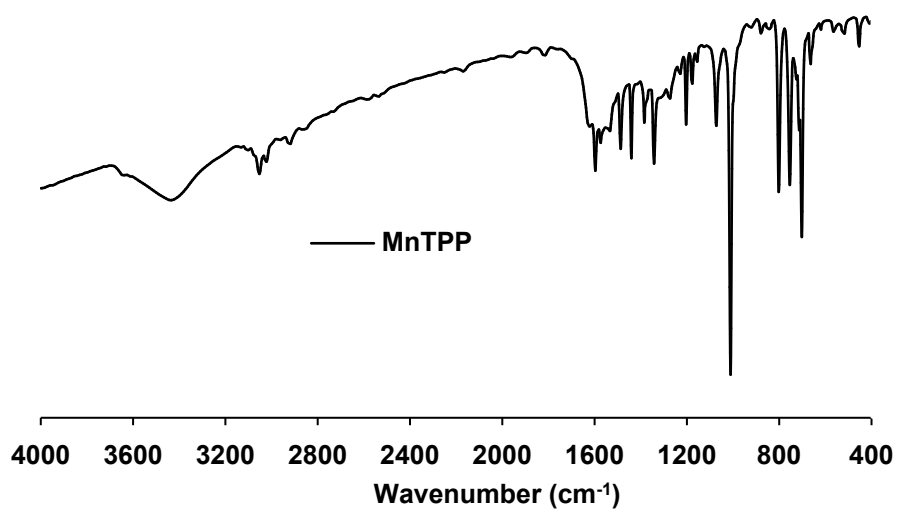**HRMS** (ESI) calculated for $C_{44}H_{28}N_4Mn$ $[M]^+$: m/z 667.16890, found 667.16770.

UV-vis (DMF) λ (ε) 437 (63850), 465 (57800), 572 (9500), 611 (8550) 680 (2400)

IR (KBr) ν (cm^{-1}) 3053, 3022, 2918, 1597, 1570, 1487, 1441, 1342, 1074, 1011, 802, 754, 702.

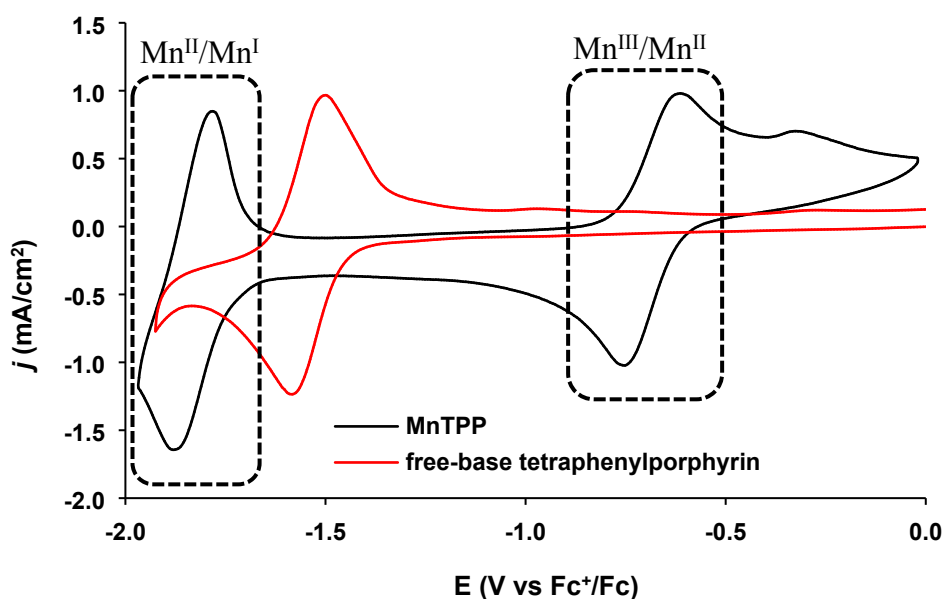m/z: 667.16890 (100.0%), 668.17225 (47.6%),
669.17561 (11.1%)

Figure S5. ESI MS spectrum of MnTPP.

Scheme S6. FTIR spectrum of MnTPP recorded in KBr disk.

4. Electrochemical behaviour of MnTPP and tetraphenylporphyrin in DMF

To determine the nature of complex electrodeposited on carbon, Mn^{III}/Mn^{II} (-0.70 V) and Mn^{II}/Mn^{I} (-1.81 V) redox waves of MnTPP were recorded (Figure S7, black trace). Additionally, CV study of free-base ligand was performed to confirm the identity of weak redox response centred around -1.60 V (Figure S7, red trace).
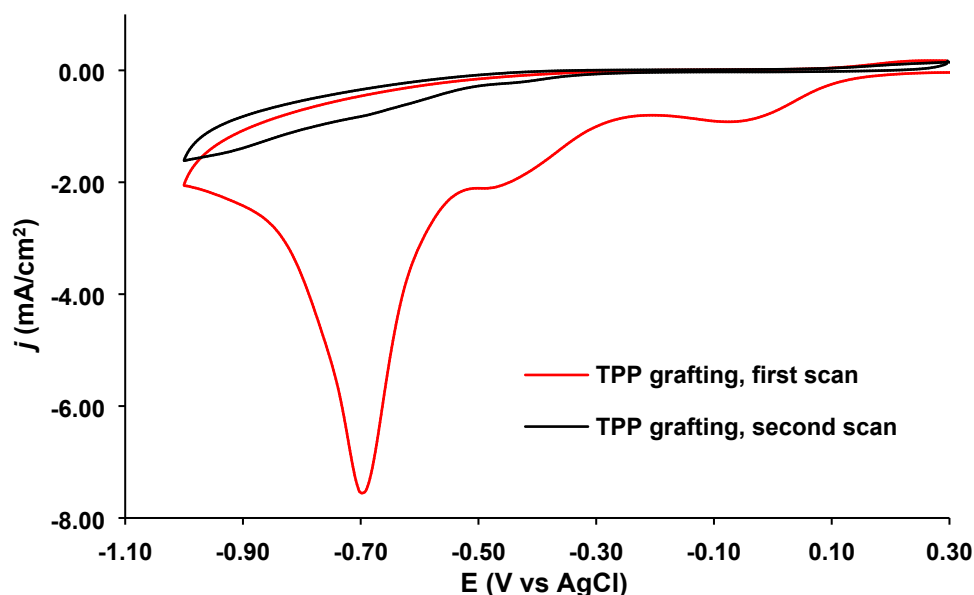

Figure S7. CVs of manganese porphyrinate (MnTPP) (black trace) and free-base tetraphenylporphyrin (red trace) recorded in dry degassed DMF electrolyte. Scan rate: 50 mV/s; TBAP concentration: 0.1 M; concentration of analytes: 2 mM.
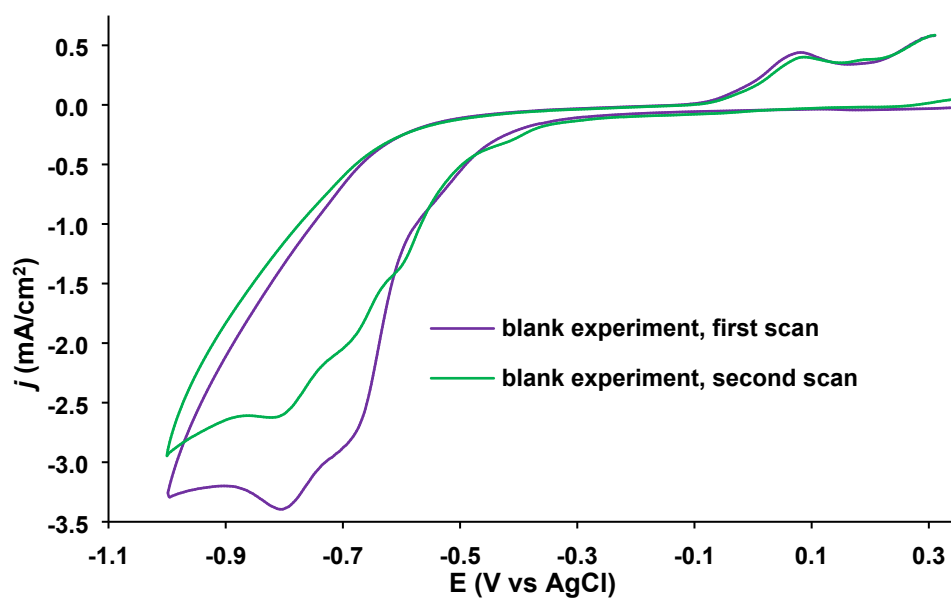
5. Determination of conditions for carbon covalent modification

Aminoporphyrin **TPP-NH$_2$** (12.6 mg, 0.02 mmol) was dissolved in 20 mL of TFA:H$_2$O (1:1) mixture in a 50 mL round-bottom flask and cooled down to -10 ºC. NaNO$_2$ (66.4 mg) was dissolved in 10 mL of deionized water and 250 µL aliquot (1.2 eqv) was added into the flask under stirring. Reaction mixture was stirred for 30 min at -10 ºC, then the septum with three electrodes was placed on top and cyclic voltammograms were recorded. Blank experiment without addition of NaNO$_2$ was performed under the same conditions. The appearance of

irreversible reduction peak around -0.05 V vs AgCl (3 M KCl) after addition of $NaNO_2$ corresponds to the reduction of $-N_2^+$ group and the formation of transient aromatic radicals attacking carbon surface (Figure S8). Notably, during the first scan insulating organic layer was formed as evidenced by the lack of significant redox responses during the second cycle (Figure S8) in strong contrast to the blank acidic solution of **TPP-NH$_2$** (Figure S9). Since overreduction of aromatic radicals upon cycling to -0.4 V vs SCE was reported by Picot et al.,[5] we opted to use more positive bias of 0.0 V vs AgCl in the potentiostatic mode for grafting of porphyrin macrocycle to the surface of carbon cloth.
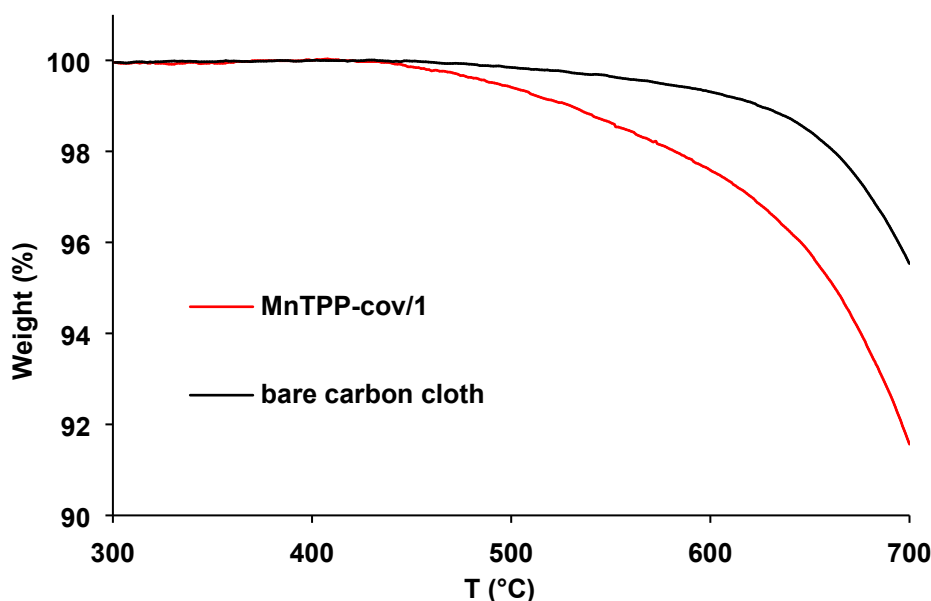

Figure S8: Cyclic voltammetry of **TPP-N$_2^+$** formed via *in situ* diazotation in TFA:H_2O (1:1).

Figure S9: Cyclic voltammetry of aminoporphyrin **TPP-NH$_2$** in TFA:H$_2$O (1:1).

6. TGA analysis of MnTPP-cov/1

Thermogravimetric analysis of **MnTPP-cov/1** showed much earlier onset of mass loss upon heating in the air. This shift was assigned to the carbon oxidation catalyzed by Mn oxides forming upon decomposition of the complex on the surface.
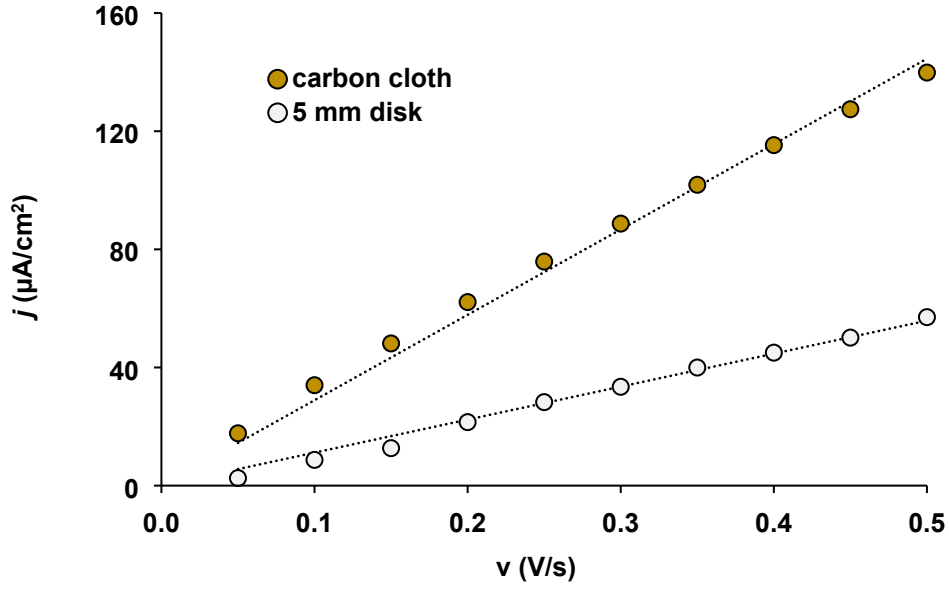

Figure S10. Thermogravimetric analysis in air of **MnTPP-cov/1** and bare carbon cloth. Heating rate 2.5 ºC min^{-1}. TGA of blank crucible was measured before each experiment and the resulting curve was subtracted.

7. Determination of relative electrochemically active surface areas for GC disk and carbon cloth

Electrochemically active surface area of carbon cloth relative to that value of GC disk electrode was determined via measurements of double layer (DL) capacitance in aqueous 0.1 $KClO_4$ at -0.39 V vs NHE where no faradic current was observed.[6] 5 mm polished glassy carbon disk electrode was used as a standard. CVs were recorded at scan rates from 0.05 to 0.5 V/s and linear correlation of capacitance current on the potential sweep rate was observed. Slopes of the graphs indicate DL capacitance values (Figure S11)

Figure S11. Anodic capacitive current densities obtained for carbon cloth and polished 5 mm glassy carbon disc electrodes.
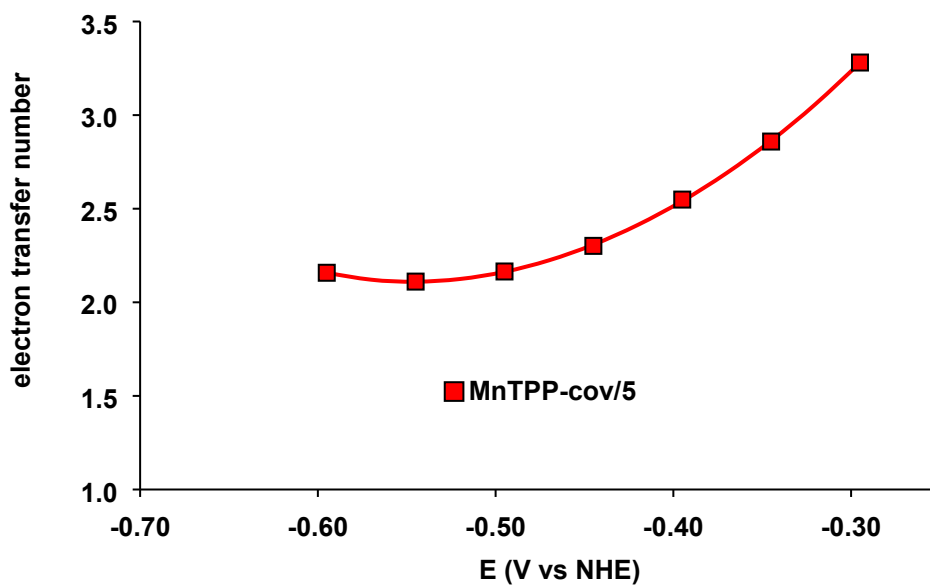
Ratio of electrochemically active surface area (S_{EA}) to geometric area (S_G) of carbon cloth was found using Equation S1:

$$S_{EA}\big/S_G = \frac{C_{carbon\ cloth}}{C_{glassy\ carbon}} = 2.6\ (\textbf{Equation S2})$$

Where $C_{carbon\ cloth}$ is DL capacitance of carbon cloth ($\mu F/cm^2$) and $C_{glassy\ carbon}$ is DL capacitance of polished glassy carbon ($\mu F/cm^2$).
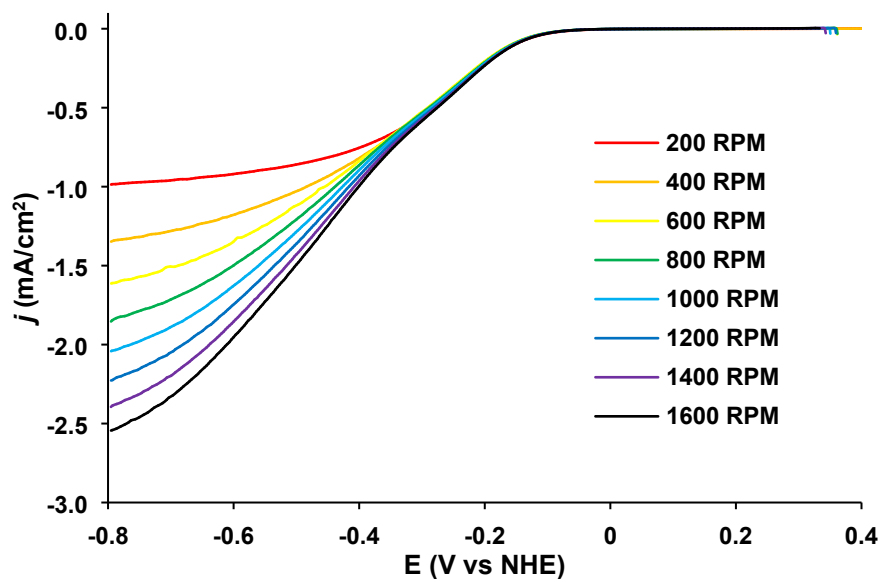
8. Dependence of ETN on electrode potential for MnTPP-cov/5 in acidic electrolyte

Figure S12. Electron transfer number observed in ORR on **MnTPP-cov/5** in acidic medium.
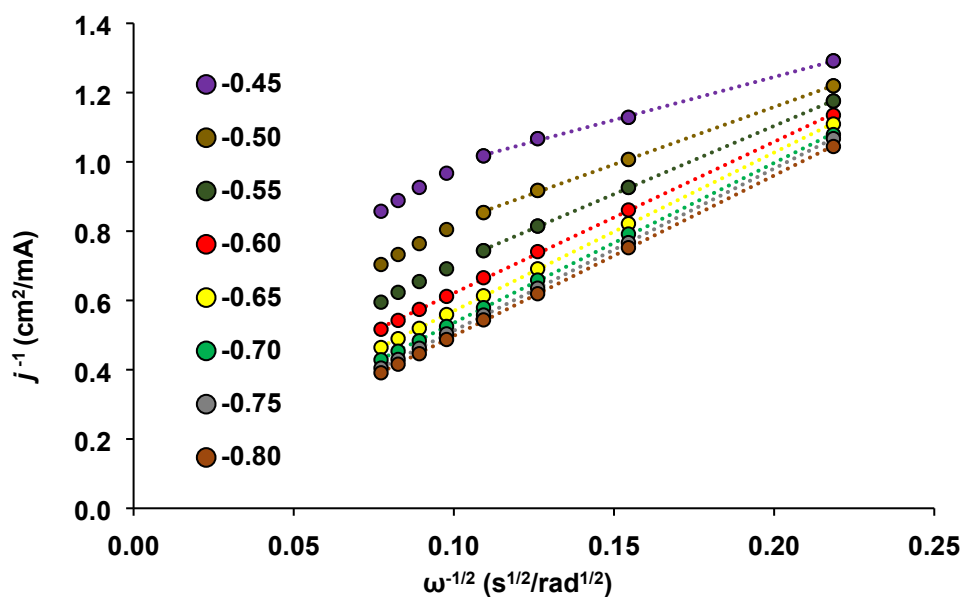
Electrolyte: O_2-saturated 0.5 M H_2SO_4.

9. LCVs of MnTPP-cov/5 in alkaline electrolyte on RDE

Figure S13. LCVs obtained for **MnTPP-cov/5** during RDE experiments in O_2-saturated
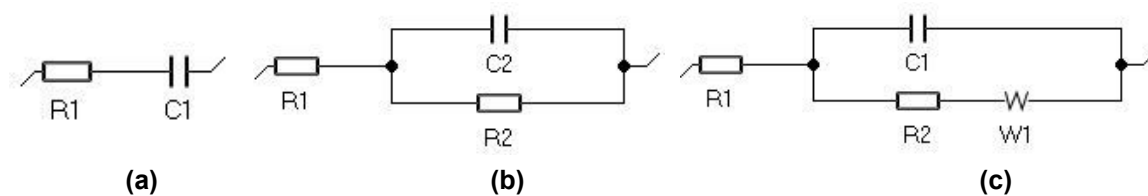
0.1 M KOH.

10. Koutecky-Levich plots of MnTPP-cov/10 in alkaline medium

Figure S14. LCVs obtained for **MnTPP-cov/5** during RDE experiments in O_2-saturated
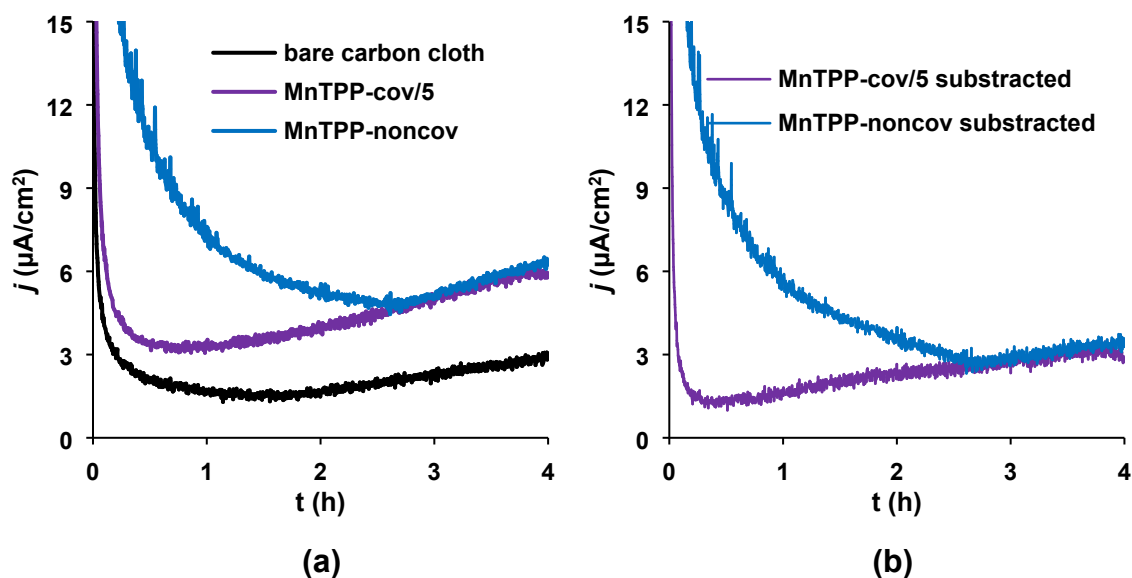
0.1 M KOH.

11. Equivalent circuits for EIS analysis

Equivalent circuits simulating EIS characteristics are presented in Figures S15 a-c.

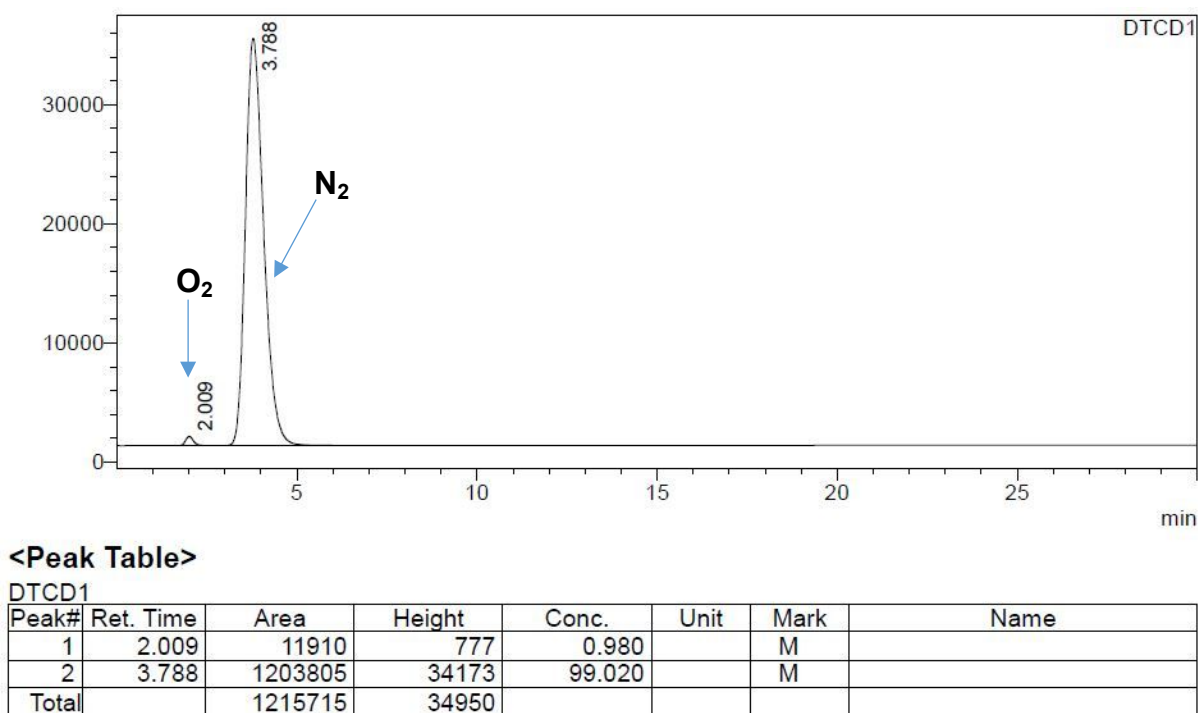**Figure S15**. Schematic representation of equivalent circuits: (a) purely capacitive coating; (b)

Randles circuit; (c) circuit containing Warburg impedance. Abbreviations: R1 - solution

resistance, R2 charge transfer impedance (resistance due to limited rate of electrochemical

reaction), C2 – capacitance of electric double layer, W1 – Warburg impedance (arising from
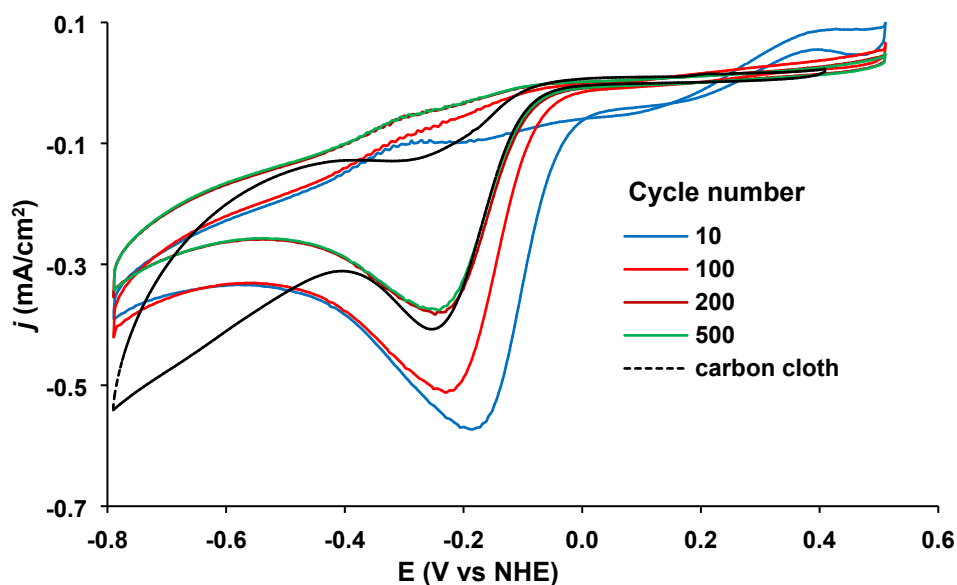
diffusion limitations).

12. Stability studies

Figure S16. (a) CPE curves for **MnTPP-noncov** (blue trace), **MnTPP-cov/5** (violet trace) and bare carbon cloth (black trace) under 1.55 V vs NHE; (b) CPE curves of **MnTPP-noncov** and **MnTPP-cov/5** with background subtracted. Electrolyte: degassed 0.5 M H_2SO_4.

<Peak Table>

DTCD1

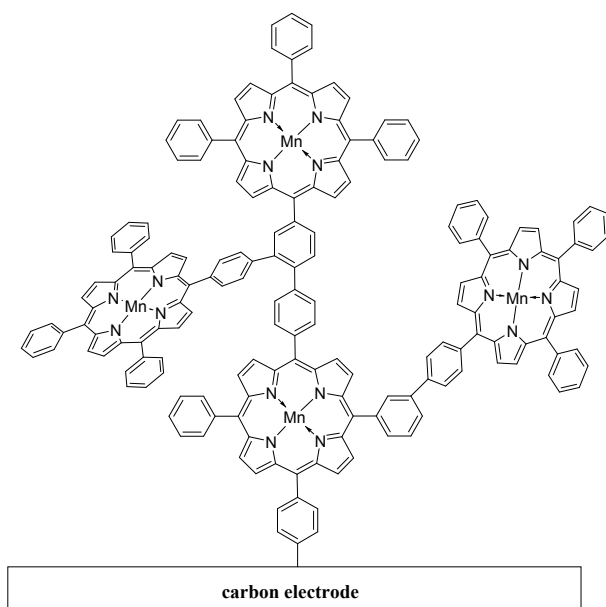| Peak#	Ret. Time	Area	Height	Conc.	Unit	Mark	Name
1	2.009	11910	777	0.980		M	
2	3.788	1203805	34173	99.020		M	
Total		1215715	34950				

Figure S17. GC analysis of anodic headspace gases after CPE on **MnTPP-cov/5**.

Figure S18. Changes in CV of **MnTPP-cov/5** upon prolonged cycling in the conditions of ORR. CV of bare carbon cloth is shown for clarity (black dotted line). Electrolyte: O_2-saturated 0.1 M KOH; scan rate: 50 mV/s.

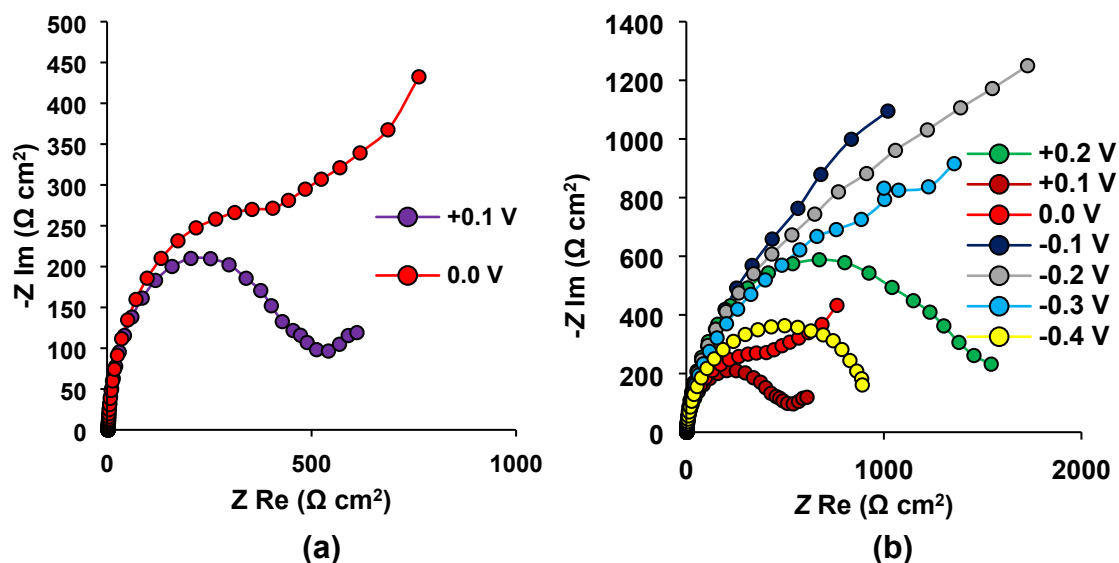## 13. Structure of MnTPP-cov/5 and MnTPP-cov/10

Figure S19. Schematic representation of **MnTPP-cov/5** and **MnTPP-cov/10** structures. Polymerization and more extensive branching of organometallic moieties is though to affect current onset compared to **MnTPP-cov/1**.
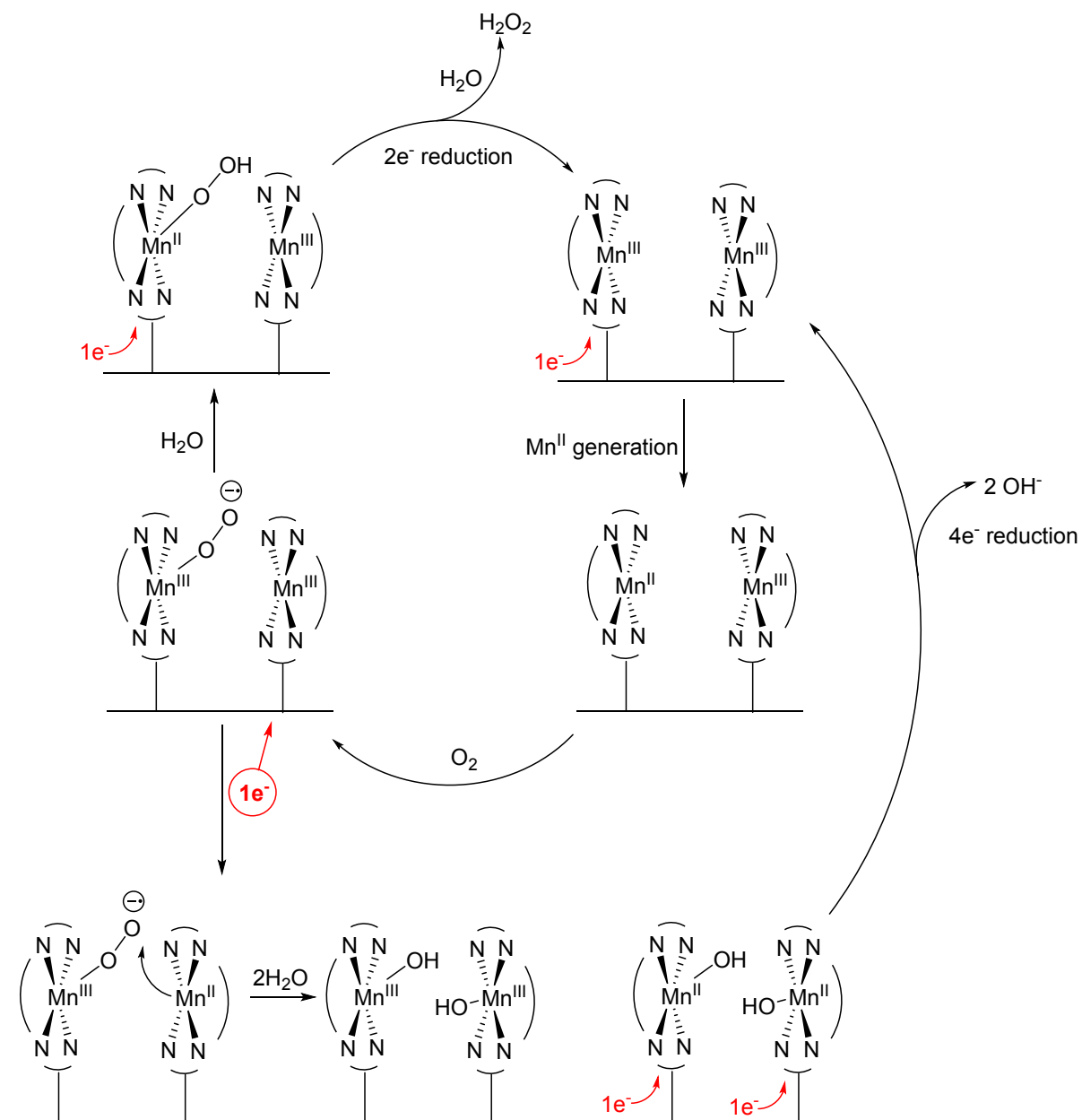
14. EIS of MnTPP-cov/5 for ORR in acidic electrolyte

Figure S20. (a) close-up view of **MnTPP-cov/5** EIS in ORR in acidic electrolyte at 0.1 and 0.0 V; (b) full impedance spectrum from -0.4 to 0.2 V.

15. Proposed ORR mechanism on Mn-Mn centers

We believe the ORR takes place as a cascade of single electron reductions coupled with proton transfers to form either H_2O_2 or H_2O as described in the Figure S21. This conclusion agrees well with the reaction mechanism proposed by G. Passard et al. for MnTPP-catalysed ORR in nonaqueous medium.[7] Even though generally ORR reactions are divided into 2e$^-$ ($O_2 \rightarrow H_2O_2$) and 4e$^-$ ($O_2 \rightarrow 2H_2O$) reductions, this notation describes overall macroscopic stoichiometry rather than actual reaction mechanism which is much more complicated.

Figure S21. Proposed mechanism of ORR catalysed by **MnTPP-cov/5** in alkaline medium.

16. References

(1) Tong, L.; Göthelid, M.; Sun, L., Oxygen evolution at functionalized carbon surfaces: a strategy for immobilization of molecular water oxidation catalysts, *Chem. Comm.* **2012,** 48 (80), 10025-10027, DOI 10.1039/C2CC35379B

(2) Adler, A. D.; Longo, F. R.; Finarelli, J. D.; Goldmacher, J.; Assour, J.; Korsakoff, L., A simplified synthesis for meso-tetraphenylporphine, *J. Org. Chem.* **1967,** 32 (2), 476-476, DOI 10.1021/jo01288a053

(3) Shi, B.; Boyle, R. W., Synthesis of unsymmetrically substituted meso-phenylporphyrins by Suzuki cross coupling reactions, *J. Chem. Soc., Perkin Trans. 1* **2002,** (11), 1397-1400, DOI 10.1039/B201622B

(4) Luguya, R.; Jaquinod, L.; Fronczek, F. R.; Vicente, M. G. H.; Smith, K. M., Synthesis and reactions of meso-(p-nitrophenyl)porphyrins, *Tetrahedron* **2004,** 60 (12), 2757-2763, DOI 10.1016/j.tet.2004.01.080

(5) Picot, M.; Nicolas, I.; Poriel, C.; Rault-Berthelot, J.; Barrière, F., On the nature of the electrode surface modification by cathodic reduction of tetraarylporphyrin diazonium salts in aqueous media, *Electrochem. Comm.* **2012,** 20, 167-170, DOI 10.1016/j.elecom.2012.04.020

(6) David, J. G.; Kumaravelu, G.; Alastair, S.; Kate, F.; Hamish, M.; Steven, P., Ultra-nanocrystalline diamond electrodes: optimization towards neural stimulation applications, *J. of Neur. Eng.* **2012,** 9 (1), 016002, DOI 10.1088/1741-2560/9/1/016002

(7) Passard, G.; Dogutan, D. K.; Qiu, M.; Costentin, C.; Nocera, D. G., Oxygen Reduction Reaction Promoted by Manganese Porphyrins, *ACS Catal.* **2018,** 8 (9), 8671-8679, DOI 10.1021/acscatal.8b01944